Jurnal Tribologi 25 (2020) 146-166

MYTRIBOS Malaysian Tribology Society

Jurnal Tribologi

Website : jurnaltribologi.mytribos.org e-issn: 2289-7232

Influence of surface roughness and pressure-dependent viscosity on load carrying mechanism in micropolar fluid squeeze film lubrication between circular stepped plates

Birendra Murmu, Pentyala Srinivasa Rao *

[1] Department of Mathematics & Computing, Indian Institute of Technology (ISM), 826004 Dhanbad, INDIA.
*Corresponding author: psrao@iitism.ac.in

KEYWORDS

Micropolar fluid
Surface roughness
Pressure-dependent viscosity
load carrying capacity
Squeeze film

ABSTRACT

In this paper, the influence of surface roughness and pressure-dependent viscosity on load carrying mechanism in micropolar fluid squeeze film lubrication between circular stepped plates is studied. The modified Reynolds equation is derived on the basis of Christensen's stochastic theory, two types of one-dimensional roughness structures, namely the radial roughness pattern and azimuthal roughness pattern is studied. It has been found that the influence of coupling parameter, viscosity parameter, non-dimensional roughness, characteristic length etc. on non-dimensional pressure, load carrying capacity and squeeze film time have been studied. It is observed that, the effect of azimuthal (radial) roughness pattern on the rough circular stepped plate increases (decreases) the load carrying capacity and the squeeze film time as compared to the corresponding smooth case. Some numerical results are also provided in tables for engineer applications.

1.0 INTRODUCTION

Eringen, (1966) presented the theory of micropolar fluids which deals with a class of fluids. These fluids can support stress movements, body movements and influenced by the spin inertia. The micropolar fluid is a subclass of these fluids which exhibit the micro rotational effects and micro rotational inertia. Eringen has gained considerable attention owing to their applications occurs in industries such as the extrusion of polymer fluids, solidification of liquid crystal, exotic

Received 10 January 2020; received in revised form 19 February 2020; accepted 5 April 2020.
To cite this article: Murmu and Rao (2020). Influence of surface roughness and pressure-dependent viscosity on load carrying mechanism in micropolar fluid squeeze film lubrication between circular stepped plates. Jurnal Tribologi 25, pp.146-166.

lubricants, animal bloods and colloidal solutions. Prakash and Sinha, (1975) studied the squeeze film theory for micropolar fluids. Several investigators have been emphasized on the use of micropolar fluid for different plates. Lin et al., (2012) studied the non-Newtonian micropolar fluid squeeze film between conical plates. Naduvinamani and Marali, (2007) studied the dynamic Reynolds equation for micropolar fluids and the analysis of plane inclined slider bearings with squeezing effect. Lin et al., (2010) also studied the effect of non-Newtonian micropolar fluid on the squeeze-film characteristics between a sphere and a plate surface. Naduvinamani and Siddangouda, (2009) analysed the squeeze film lubrication between circular stepped plates of couple stress fluids.

Generally, the asperity height of surface roughness is same order as the mean separation between lubricated contacts. In this circumstance, effects of surface roughness on the performance of the bearing system must be considered. Many researchers have examined the effect of surface roughness on the squeeze film of various bearing systems by using micropolar fluid theory. Shukla and Isa, (1975) derived the generalised Reynolds equation for micropolar lubricants. Using stochastic model, Christensen, (1969) investigated the hydrodynamic lubrication of rough surfaces. Christensen and Tonder, (1971) proposed a new stochastic averaging approach for the study of roughness effects on the hydrodynamic lubrication. Naduvinamani et al., (2010) extended the application of micropolar fluid theory of inclined stepped composite bearings with rough surfaces. Siddangouda et al., (2017) studied the effects of piezo-viscous and surface roughness on the squeeze film characteristics of micropolar fluid in convex curved plates. It is found that, when the viscosity variation parameter increases then squeeze film pressure decreases and also effect of pressure-dependent viscosity increases with increase in value of amplitude ratio parameter in both radial and azimuthal roughness. The squeeze film time decreases when the viscosity variation parameter increases. Rao et al., (2017) studied the effect of surface roughness and non-Newtonian micropolar fluid squeeze film between conical bearings. Elsharkawy and Al-Fadhalah, (2011) studied the effect of the permeability and surface roughness on the squeeze film characteristics of non-Newtonian behaviour of micropolar fluid on rigid sphere and porous flat surface. Naduvinamani et al., (2010) studied the effect of surface roughness on the squeeze fluid film characteristics of short porous partial journal bearings lubricated with micropolar fluid. Hanumagowda, (2015) studied the combined effect of pressure-dependent viscosity and couple stress on squeeze film lubrication between circular step plates. He extended his work Hanumagowda et al., (2018) to incorporate the effect of surface roughness and pressure-dependent viscosity over couple stress squeeze film lubrication between circular stepped plates. Naduvinamani et al., (2012) studied the combined effects of MHD and surface roughness on the couple stresses squeeze film lubrication between circular stepped plates.

The relation between viscosity and pressure is analysed by the following relation Barus, (1893), Bartz and Ether, (2008).

$$\mu = \mu_0 e^{\beta p} \tag{1}$$

Where β denotes the coefficient of pressure dependent viscosity (PDV) and μ_0 is the viscosity at ambient pressure and a constant temperature. Equation (1) indicates the lubricant viscosity is increasing exponentially and it could alter the predicted performance of squeeze film bearings. Naduvinamani et al., (2015) studied the effect of pressure dependent viscosity on squeeze film characteristics of micropolar fluid in convex curved plates. Hanumagowda et al., (2018) also studied the effect of pressure dependent viscosity on couple stress squeeze film lubrication between porous circular stepped plates.

In the present article, we extend the work of Hanumagowda et al., (2016) to incorporate the influence of surface roughness and pressure-dependent viscosity on load carrying mechanism in micropolar fluid squeeze film lubrication between circular stepped plates. The modified Reynolds equation is derived on the basis of micropolar fluid theory. The effect of surface roughness on pressure, load-carrying capacity and squeeze film time are obtained.

2.0 MATHEMATICAL FORMULATION OF THE PROBLEM

Squeeze film between two rough circular stepped plates approaching each other with squeezing velocity $V(=\partial H/\partial t)$, where H is the film thickness between the two plates. The geometry and coordinates of the problem under consideration is shown in Figure 1. The constitutive equations for micropolar fluid proposed by Eringen, (1966) simplify considerably under the usual assumptions of hydrodynamic lubrication theory for thin films Pinkus and Sternlicht, (1961) are

Conservation of linear momentum: $$\left(\mu+\frac{\chi}{2}\right)\frac{\partial^2 u}{\partial y^2}+\chi\frac{\partial v_3}{\partial y}-\frac{\partial p}{\partial r}=0 \tag{2}$$

Conservation of angular momentum: $$\gamma\frac{\partial^2 v_3}{\partial y^2}-2\chi v_3-\chi\frac{\partial u}{\partial y}=0 \tag{3}$$

Conservation of mass: $$\frac{1}{r}\frac{\partial}{\partial r}(ru)+\frac{\partial v}{\partial y}=0 \tag{4}$$

where u,v are the velocity components of the lubricant in the r and y directions, respectively, v_3 is the micro rotational velocity component, χ is the spin viscosity, γ is the viscosity coefficient for micropolar fluids and μ is the Newtonian viscosity coefficient.

The relevant boundary conditions for the velocity and micro rotational velocity components are

At the upper surface $(y=H)$

$$u=0,\ v=\frac{\partial H}{\partial t},\ v_3=0 \tag{5a}$$

At the bearing surface $(y=0)$

$$u=0,\ v=0,\ v_3=0 \tag{5b}$$

The fluid film thickness H is defined by

$$H = h_1 \text{ for } 0 \le r \le KR$$
$$= h_2 \text{ for } KR \le r \le R \text{ with } 0 \le K \le 1$$

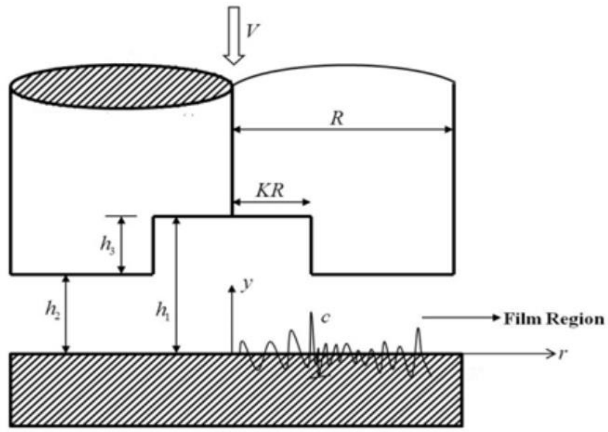

Figure. 1 Squeeze film between rough circular stepped plates.

3.0 SOLUTION OF THE PROBLEM

The solution of equations (2) and (3) subject to corresponding boundary conditions (5a) and (5b) are obtained in the form:

$$u = \frac{y}{2\mu_0 e^{\beta p}}\frac{\partial p}{\partial r}(y-H) + \frac{N^2}{m}\frac{H}{2\mu_0 e^{\beta p}}\frac{\partial p}{\partial r}\left[\sinh my - \frac{(\cosh mH + 1)(\cosh my - 1)}{\sinh mH}\right] \quad (6)$$

$$v_3 = \frac{D_1 \sinh my}{2(1-N^2)}\left[\frac{(\cosh my - 1)}{\sinh my} - \frac{(\cosh mH - 1)}{\sinh mH}\right] + \frac{H}{2\mu_0 e^{\beta p}}\frac{\partial p}{\partial r}\left[\frac{\sinh my}{\sinh mH} - \frac{y}{H}\right] \quad (7)$$

Where,

$$D_1 = -\frac{(1-N^2)}{2}\frac{H}{\mu_0 e^{\beta p}}\frac{\partial p}{\partial r}, \text{ and } m = \frac{N}{l}, \; N = \left(\frac{\chi}{\chi + 2\mu}\right)^{1/2}, \; l = \left(\frac{\gamma}{4\mu}\right)^{1/2}.$$

The modified Reynolds equation for the pressure in the film region is obtained by using equations (6) in integrating the continuity equation (4) with respect to y over the film thickness, H and also using the boundary conditions for v given in equations (5a) and (5b) in the form:

$$\frac{\partial}{\partial r}\left[f(N, l, H)e^{-\beta p} r \frac{\partial p}{\partial r}\right] = 12 r \mu_0 \frac{\partial H}{\partial t} \quad (8)$$

Where,

$$f\left(N,\, l,\, H\right)=H^{3}+12l^{2}H-6NlH^{2}\coth\left(\frac{NH}{2l}\right)$$

The volume flow rate of the lubricant is given by

$$Q=2\pi r\int_{0}^{H}udy \tag{9}$$

Substituting the expression for u from equation (6) in equation (9) the volume flux is obtained in the form

$$Q=-\frac{\pi re^{-\beta p}}{6\mu_{0}}\frac{\partial p}{\partial r}f\left(N,\, l,\, H\right) \tag{10}$$

To mathematically model the surface roughness, the fluid film thickness is considered to be made up of two parts

$$H_{i}=h_{i}+h_{s}\left(r,\theta,\xi\right) \tag{11}$$

Let $f\left(h_{s}\right)$ be the probability density function of the stochastic film thickness h_{s}. Taking the stochastic average of modified Reynolds equation (8) with respect to $f\left(h_{s}\right)$, the stochastic modified Reynolds equation is obtained in the form

$$\frac{\partial}{\partial r}\left[E\left(f\left(N,\, l,\, H\right)\right)e^{-\beta E(p)}r\frac{\partial E(p)}{\partial r}\right]=12r\mu_{0}\frac{\partial E(H)}{\partial t} \tag{12}$$

Where,

$$E(\bullet)=\int_{-\infty}^{\infty}(\bullet)f(h_{s})dh_{s} \tag{13}$$

For most of the lubricating surfaces, the Gaussian distribution for describing the roughness profile heights is valid up to at least three standard deviations. Following Christensen, the roughness distribution function is assumed in the following form

$$f(h_{s})=\begin{cases}\dfrac{35}{32c^{7}}(c^{2}-h_{s}^{2})^{3} & if \quad -c\leq h_{s}\leq c\\ 0 & \text{elsewhere}\end{cases} \tag{14}$$

Where $c = 3\bar{\sigma}$ and $\bar{\sigma}$ is the standard deviation.

In the context of Christensen's stochastic theory for the hydrodynamic lubrication of rough surfaces, two types of one-dimensional roughness patterns are considered namely the radial roughness pattern and the azimuthal roughness pattern.

3.1 Radial Roughness Pattern

The one-dimensional radial roughness pattern has the form of long, narrow ridges and valleys running in the radial direction (i.e. they are straight ridges and valley passing through $y = 0, r = 0$ to form star pattern), in this case the film thickness takes the form

$$H_i = h_i + h_s\left(\theta, \xi\right) \tag{15}$$

And the average modified Reynolds equation (12) takes the form

$$\frac{\partial}{\partial r}\left[E\left(f\left(N,\, l,\, H\right)\right)e^{-\beta E(p)} r \frac{\partial E(p)}{\partial r}\right] = 12 r \mu_0 \frac{\partial E(H)}{\partial t} \tag{16}$$

3.2 Azimuthal Roughness Pattern

The one-dimensional azimuthal roughness pattern on the bearing surface has the roughness structure in the form of long narrow ridges and valleys running in θ-direction (i.e. they are circular ridges and valleys on the flat plate that are concentric on $y = 0, r = 0$), in this case the film thickness assumes the form

$$H_i = h_i + h_s\left(r, \xi\right) \tag{17}$$

and the averaged modified Reynolds equation (12) takes the form

$$\frac{\partial}{\partial r}\left[\frac{e^{-\beta E(p)}\ r}{E\left(1/f\left(N,\, l,\, H\right)\right)} \frac{\partial E(p)}{\partial r}\right] = 12 r \mu_0 \frac{\partial E(H)}{\partial t} \tag{18}$$

Equations (16) and (18) together can be written as

$$\frac{\partial}{\partial r}\left[g_i\left(N,\, l,\, H_i,\, c\right)e^{-\beta E(p)}\ r \frac{\partial E(p)}{\partial r}\right] = 12 r \mu_0 \frac{\partial E(H)}{\partial t} \tag{19}$$

Where,

$$g_i\left(N, l, H_i,\, c\right) = \begin{cases} E\left[\,f_i\left(N, l, H_i\right)\right] & \text{for radial roughness} \\ E\left[1/f_i\left(N, l, H_i\right)\right]^{-1} & \text{for azimuthal roughness} \end{cases}$$

and $f_i\left(N,l,H_i\right)=H_i^3+12l^2H_i-6NlH_i^2\coth\left(\frac{NH_i}{2l}\right)$

using the non- dimensional quantities

$$H_i^*=\frac{H_i}{h_0},\quad h_1^*=\frac{h_1}{h_0},\quad h_s^*=\frac{h_s}{h_0},\quad r^*=\frac{r}{R},\quad l^*=\frac{l}{h_0},\quad c^*=\frac{c}{h_0},\quad P^*=\frac{E(p)h_0^3}{\mu_0R^2\left(-\partial h/\partial t\right)}$$

$$G=\frac{\beta\mu_0R^2\left(-\partial h/\partial t\right)}{h_0^3},\quad Q^*=\frac{Q}{R^2\left(-\partial h/\partial t\right)}$$

In equations (10) and (19) the non- dimensional volume flow rate and Reynolds equation are obtained in the form

$$\frac{\partial}{\partial r^*}\left[g_i^*\left(N,\,l^*,\,H_i^*,\,c^*\right)e^{-GP^*}r^*\frac{\partial P^*}{\partial r^*}\right]=-12r^* \tag{20}$$

$$Q^*=-\frac{\pi r^*e^{-GP^*}}{6}\frac{\partial P^*}{\partial r^*}g_i^*\left(N,l^*,H_i^*\right) \tag{21}$$

where

$$g_i^*\left(N,l^*,H_i^*,\,c^*\right)=\begin{cases}E\left[f_i^*\left(N,l^*,H_i^*\right)\right] & \text{for radial roughness}\\ E\left[1/f_i^*\left(N,l^*,H_i^*\right)\right]^{-1} & \text{for azimuthal roughness}\end{cases}$$

and $f_i^*\left(N,l^*,H_i^*\right)=H_i^{*3}+12l^{*2}H_i^*-6Nl^*H_i^{*2}\coth\left(\frac{NH_i^*}{2l^*}\right)$

Reynolds equations in region I: $\left(0\le r^*\le K\right)$

$$\frac{\partial}{\partial r^*}\left[g_1^*\left(N,\,l^*,\,H_1^*,\,c^*\right)e^{-GP_1^*}r^*\frac{\partial P_1^*}{\partial r^*}\right]=-12r^* \tag{22}$$

Reynolds equations in region II: $\left(K\le r^*\le 1\right)$

$$\frac{\partial}{\partial r^*}\left[g_2^*\left(N,\,l^*,H_2^*,\,c^*\right)e^{-GP_2^*}r^*\frac{\partial P_2^*}{\partial r^*}\right]=-12r^* \tag{23}$$

where

$$g_i^*\left(N,l^*,H_i^*,\,c^*\right)=\begin{cases}E\left[f_i^*\left(N,l^*,H_i^*\right)\right] & \text{for radial roughness}\\ E\left[1/f_i^*\left(N,l^*,H_i^*\right)\right]^{-1} & \text{for azimuthal roughness}\end{cases}$$

$$f_1^*\left(N,l^*,H_1^*\right)=H_1^{*3}+12l^{*2}H_1^*-6Nl^*H_1^{*2}\coth\left(\frac{NH_1^*}{2l^*}\right)$$

$$f_2^*\left(N,l^*,H_2^*\right)=H_2^{*3}+12l^{*2}H_2^*-6Nl^*H_2^{*2}\coth\left(\frac{NH_2^*}{2l^*}\right)$$

$$H_1^*=h_1^*+h_s^*,\ \ H_2^*=1+h_s^*$$

The relevant boundary conditions for the pressure

$$\frac{dP_1^*}{dr^*}=0 \quad \text{at } r^*=0 \tag{24}$$

$$P_2^*=0 \quad \text{at } r^*=1 \tag{25}$$

$$P_1^*=P_2^* \quad \text{at } r^*=K \tag{26}$$

$$Q_1^*=Q_2^* \quad \text{at } r^*=K \tag{27}$$

where Q_1^* is the non-dimensional volume flow rate in region I and Q_2^* is the non-dimensional volume flow rate in region II.

Solving equations (22) and (23) using the boundary conditions (24), (25), (26) and (27) gives

Pressure in region I: $\left(0\le r^*\le K\right)$

$$P_1^*=-\frac{1}{G}\,\mathrm{In}\left\{\frac{3G\left(r^{*2}-K^2\right)}{g_1^*\left(N,l^*,H_1^*,\,c^*\right)}+\frac{3G\left(K^2-1\right)}{g_2^*\left(N,l^*,H_2^*,\,c^*\right)}+1\right\} \tag{28}$$

Pressure in region II: $\left(K\le r^*\le 1\right)$

$$P_2^*=-\frac{1}{G}\,\mathrm{In}\left\{\frac{3G\left(r^{*2}-1\right)}{g_2^*\left(N,l^*,H_2^*,\,c^*\right)}+1\right\} \tag{29}$$

The load carrying capacity is obtained in the following form:

$$E(w)=2\pi\int_0^{KR} rp_1dr+2\pi\int_{KR}^{1} rp_2dr \tag{30}$$

The non-dimensional load carrying capacity is obtained in the form

$$W^*=\frac{E(w)h_0^3}{\mu_0R^4\left(-dh/dt\right)}=2\pi\int_0^K r^*P_1^*dr^*+2\pi\int_K^1 r^*P_2^*dr^*$$

$$W^*=-\frac{2\pi}{G}\left\{\int_0^K \mathrm{In}\left\{\frac{3G\left(r^{*2}-K^2\right)}{g_1^*\left(N,l^*,H_1^*,\,c^*\right)}+\frac{3G(K^2-1)}{g_2^*\left(N,l^*,H_2^*,\,c^*\right)}+1\right\}r^*dr^*+\int_K^1 \mathrm{In}\left\{\frac{3G\left(r^{*2}-1\right)}{g_2^*\left(N,l^*,H_2^*,\,c^*\right)}+1\right\}r^*dr^*\right\} \tag{31}$$

The squeezing time for reducing the film thickness from an initial value $H_2^*=1$ to a final value h_f^* is given by

$$T^*=\frac{E(w)\,t\,h_0^2}{\mu_0R^4}$$

$$T^{*}=-\frac{2\pi}{G}\int_{h_f^*}^{1}\int_{0}^{K}\text{In}\left\{\frac{3G\left(r^{*2}-K^{2}\right)}{g_1^*\left(N,l^*,H_1^*,c^*\right)}+\frac{3G(K^{2}-1)}{g_2^*\left(N,l^*,H_2^*,c^*\right)}+1\right\}r^{*}dr^{*}dh_2$$
$$-\frac{2\pi}{G}\int_{h_f^*}^{1}\frac{2\pi}{G}\int_{K}^{1}\text{In}\left\{\frac{3G\left(r^{*2}-1\right)}{g_2^*\left(N,l^*,H_2^*,c^*\right)}+1\right\}r^{*}dr^{*}dh_2 \qquad (32)$$

where

$$H_1^*=h_2^*+h_3^*+h_s^*,\ H_2^*=h_2^*+h_s^*,\ h_2^*=\frac{h_2}{h_0},\ h_3^*=\frac{h_3}{h_0},\ h_s^*=\frac{h_s}{h_0},\ h_f^*=\frac{h_f}{h_0},\ l^*=\frac{l}{h_0}$$

4.0 RESULTS AND DISCUSSION

The variation of non-dimensional pressure P^* with r^* for different values of G with $l^*=0.3,\ h_1^*=1.2,\ K=0.7,$ and $c^*=0.1$ for two values of coupling parameter $N=0.0$ and 0.3 is shown in Figure 2 for both types of roughness patterns. It is observed that the effect of viscosity parameter is to increase the squeeze film pressure for both radial as well as azimuthal roughness patterns. Figure 3 shows the variation of non-dimensional pressure P^* with r^* for different values of c^* with $l^*=0.3,\ h_1^*=1.2,\ K=0.7,\ N=0.3$ and $G=0.04$ for both types of roughness patterns. It is observed that the pressure P^* decreases with increase in c^* for radial roughness pattern, whereas P^* increases with increase in the values of c^* for azimuthal roughness pattern. The variation of pressure P^* with r^* for different values of coupling number N with $l^*=0.3,\ h_1^*=1.2,\ K=0.7,\ G=0.04$ and $c^*=0.1$ is depicted in Figure 4 for both types of roughness patterns. It is observed that the effect of N is to increase P^* as compared to the Newtonian case for both types of roughness patterns. Further, the increase in P^* is more pronounced for the azimuthal roughness pattern as compared to radial roughness pattern..

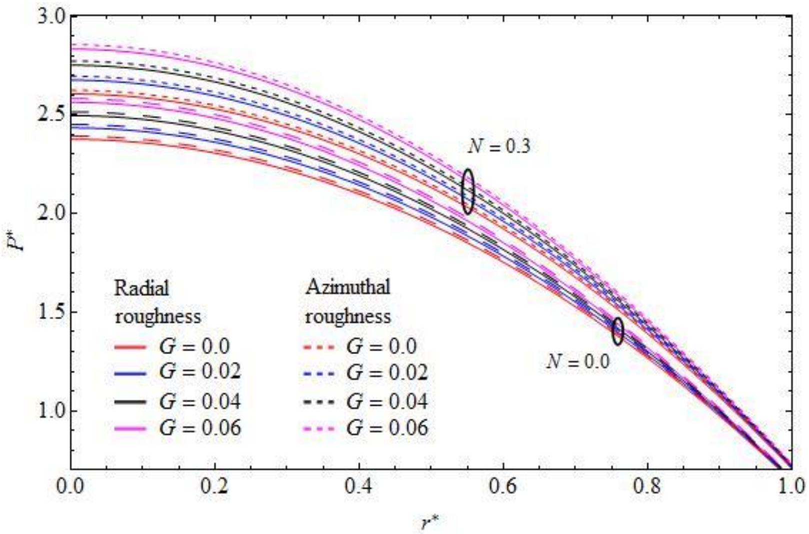

Figure 2: Variation of non-dimensional pressure P^* with r^* for different values of G and N with $l^* = 0.3,\ h_1^* = 1.2,\ K = 0.7,\ c^* = 0.1$.

Table 1: Numerical comparison between the results of Hanumagowda, (2016) and the present analysis (with $c^* = 0$) with $l^* = 0.3, N = 0.3,$ $K = 0.6$ and $h_3^* = 0.2$.

I. Load carrying capacity W^*

	$h_1^* = 1.5$					$h_1^* = 2.0$				
		Present analysis					Present analysis			
		$c^* = 0$		$c^* = 0.3$			$c^* = 0$		$c^* = 0.3$	
G	**Hanumagowda, (2016)**	**Radial**	**Azimuthal**	**Radial**	**Azimuthal**	**Hanumagowda, (2016)**	**Radial**	**Azimuthal**	**Radial**	**Azimuthal**
0.00	4.69629	4.69629	4.69629	4.60536	4.93775	4.58156	4.58156	4.58156	4.49235	4.81915
0.02	4.78705	4.78705	4.78705	4.69260	5.03817	4.66688	4.66688	4.66688	4.57434	4.91365
0.04	4.88361	4.88361	4.88361	4.78532	5.14534	4.75743	4.75743	4.75743	4.66127	5.01424
0.06	4.98612	4.98612	4.98612	4.88362	5.25948	4.85329	4.85329	4.85329	4.75319	5.12108

II. Squeeze film time T^*

	$h_1^* = 0.6$					$h_1^* = 0.8$				
		Present analysis					Present analysis			
		$c^* = 0$		$c^* = 0.3$			$c^* = 0$		$c^* = 0.3$	
G	**Hanumagowda, (2016)**	**Radial**	**Azimuthal**	**Radial**	**Azimuthal**	**Hanumagowda, (2016)**	**Radial**	**Azimuthal**	**Radial**	**Azimuthal**
0.00	4.29475	4.29475	4.29475	4.23026	4.61191	1.36860	1.36860	1.36860	1.34049	1.45295
0.02	4.54014	4.54014	4.54014	4.46927	5.89894	1.40995	1.40995	1.40995	1.38012	1.49975
0.04	4.84558	4.84558	4.84558	4.76629	5.26438	1.45564	1.45564	1.45564	1.42382	1.55182
0.06	5.24923	5.24923	5.24923	4.15789	5.76802	1.50631	1.50631	1.50631	1.47216	1.61003

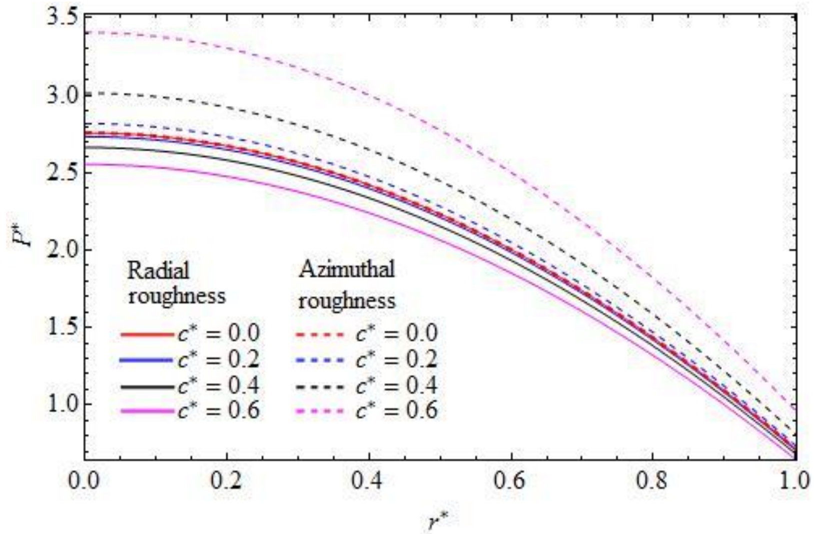

Figure 3: Variation of non-dimensional pressure P^* with r^* for different values of c^* with $l^* = 0.3,\ h_1^* = 1.2,\ K = 0.7,\ N = 0.3, G = 0.04$

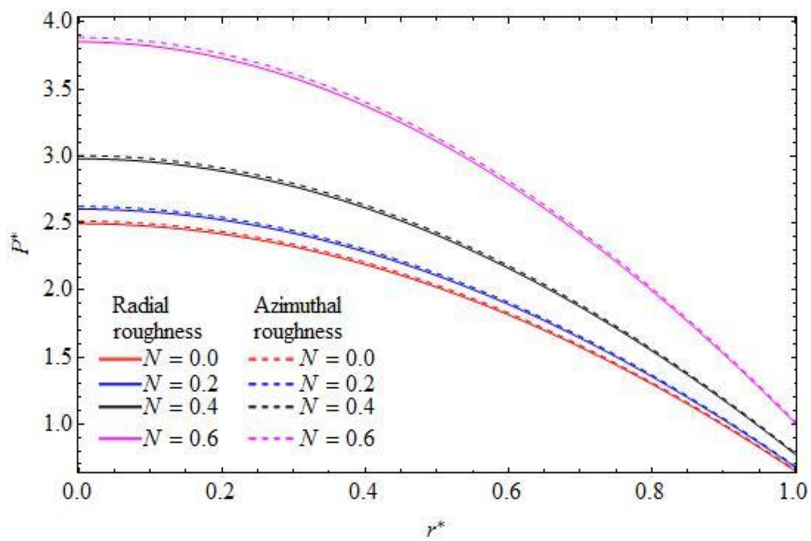

Figure 4: Variation of non-dimensional pressure P^* with r^* for different values of N with $l^* = 0.3,\ h_1^* = 1.2,\ K = 0.7,\ G = 0.04, c^* = 0.1$.

Figure 5 shows the variation of pressure P^* with r^* for different values of l^* with $h_1^* = 1.2,\ K = 0.7,\ G = 0.04,\ N = 0.3$ and $c^* = 0.1$ for both types of roughness patterns. It is observed that the non-dimensional pressure increases with increasing values of l^*. Further, the increase in P^* is more pronounced for the azimuthal roughness pattern as compared to the radial roughness pattern. It is observed that the effect of azimuthal roughness pattern is to increase the fluid film pressure. The variation of non-dimensional maximum pressure P^*_{max} with K for different values of roughness parameter c^* with $l^* = 0.3$, $h_1^* = 1.2$, $G = 0.04$ and $N = 0.3$ is show in Figure 6 for both types of roughness patterns. It is observed that the maximum pressure P^*_{max} decreases with increasing values of c^* for radial roughness pattern, whereas maximum pressure P^*_{max} increases with increase in values of c^* for azimuthal roughness pattern.

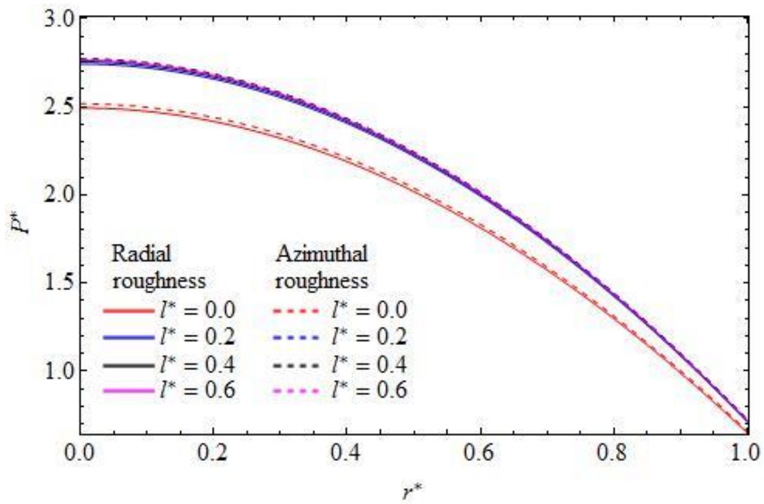

Figure 5: Variation of non-dimensional pressure P^* with r^* for different values of l^* with $h_1^* = 1.2$, $K = 0.7$, $G = 0.04$, $N = 0.3, c^* = 0.1$.

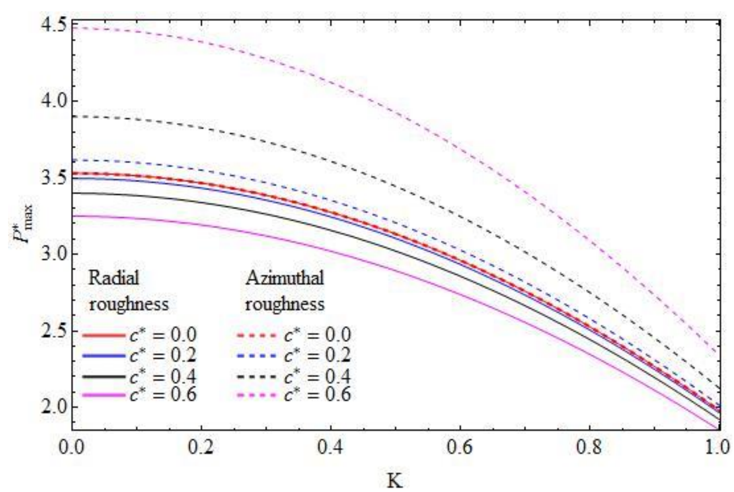

Figure 6: Variation of non-dimensional maximum pressure P^*_{max} with K for different values of c^* with $l^* = 0.3$, $h_1^* = 1.2$, $G = 0.04, N = 0.3$.

4.2 Load-Carrying Capacity

Figures 7 to 11 shows the variation of non-dimensional load carrying capacity W^* with h_1^* for different values of G, N and l^* for fixed K. It is observed that the non-dimensional load carrying capacity W^* decreases with increasing values of h_1^*. The load carrying capacity is more for azimuthal roughness compared to radial roughness case. It is also observed that the non-dimensional load carrying capacity increases for increasing values of G, N and l^*. Figure 8 shows that the load carrying capacity W^* increases (decreases) for increasing values of c^* for the azimuthal (radial) roughness. The variation of non-dimensional load carrying capacity W^* with K is shown in Figure 10. It is observed that the non- dimensional load carrying capacity decreases with increasing values of K.

The relative percentage increase in the non-dimensional load carrying capacity R_{W^*} is defined by $R_{W^*} = \left\{ \left(W^*_{PDV} - W^*_{Non-PDV} \right) / W^*_{Non-PDV} \right\} \times 100$. Table 2 shows the variation of R_{W^*} for different values G and c^* with l^*, N, K and h_1^*.

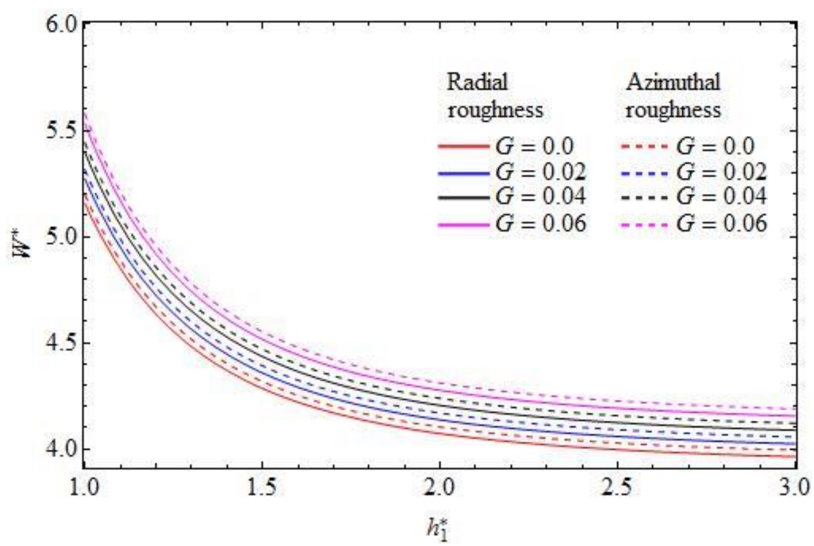

Figure 7: Variation of non-dimensional load carrying capacity W^* with h_1^* for different value of G with $l^* = 0.3, K = 0.7, N = 0.3, c^* = 0.1$.

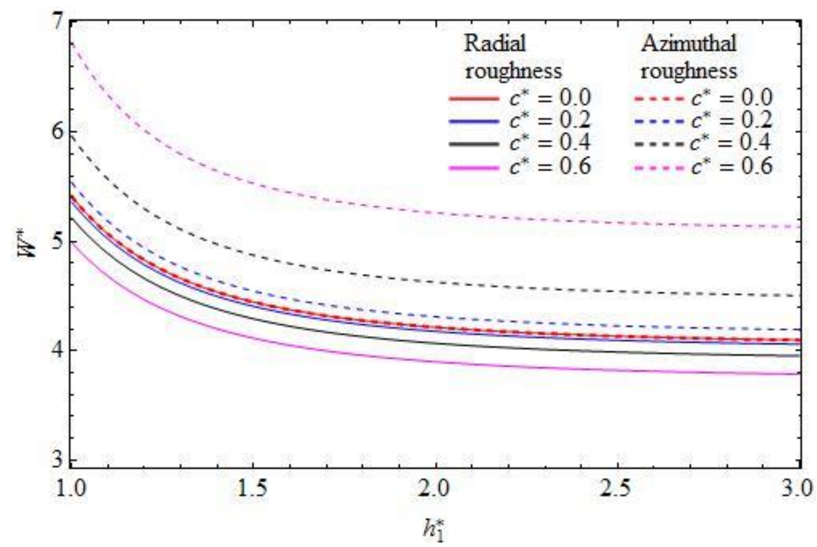

Figure 8: Variation of non-dimensional load carrying capacity W^* with h_1^* for different values of c^* with $l^* = 0.3, K = 0.7, G = 0.04, N = 0.3$.

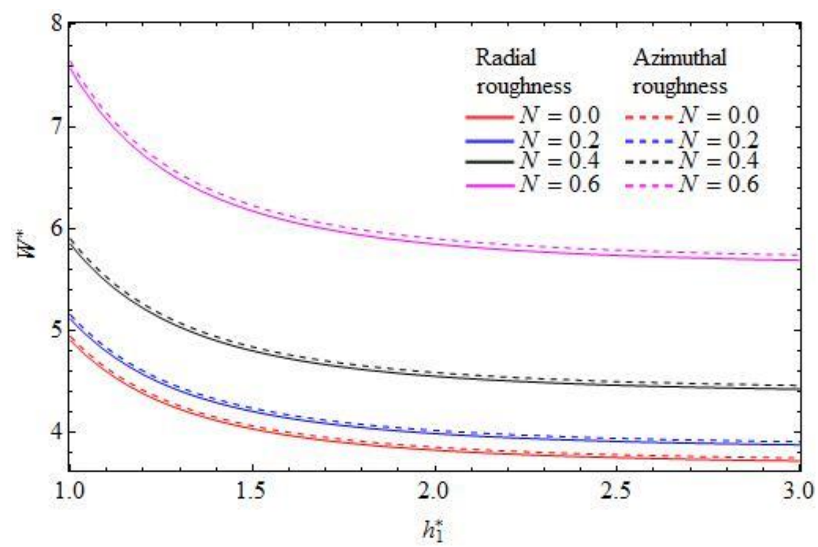

Figure 9: Variation of non-dimensional load carrying capacity W^* with h_1^* for different values of N with $l^* = 0.3, K = 0.7, \mathrm{G} = 0.04, c^* = 0.1$.

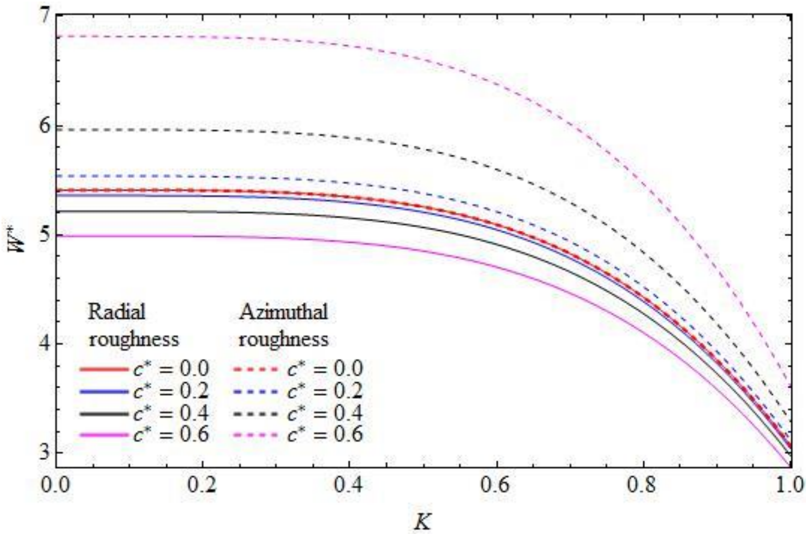

Figure 10: Variation of non-dimensional load carrying capacity W^* with K for different values of c^* with $l^* = 0.3, h_1^* = 1.2, \mathrm{G} = 0.04, N = 0.1$.

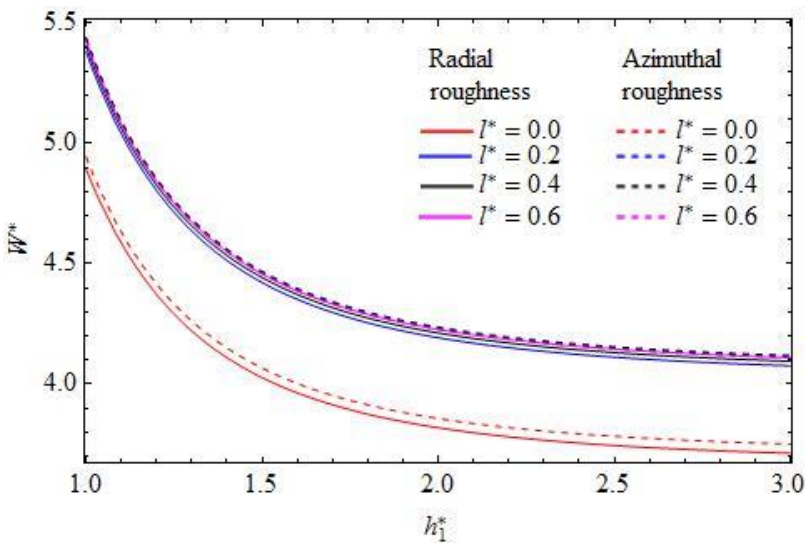

Figure 11: Variation of non-dimensional load carrying capacity W^* with h_1^* for different values of l^* with $\mathrm{G} = 0.04, \mathrm{N} = 0.3, \mathrm{K} = 0.7, c^* = 0.1$.

4.3 Squeeze Film Time

The variation of non-dimensional squeeze film time T^* with h_f^* for different values of G and N for fixed K is shows in Figure 12 to 15. It is observed that as values of h_f^* increases, decrease in non-dimensional squeeze film time T^* is observed. Further, it is observed that the non-dimensional squeeze film time T^* increases, for increasing values of G and N. Figure 13 shows the variation of non-dimensional squeeze film time T^* for radial roughness and more for the azimuthal roughness. Figure 15 shows the variation of non-dimensional squeeze film time T^* with K for different values of c^*. It is also observed that the effect of azimuthal (radial) roughness pattern is to increase (decrease) non-dimensional squeeze film time T^* for increasing values of c^*.

The relative percentage increase in the non-dimensional squeeze film time R_{T^*} is defined by $R_{T^*} = \left\{ \left(T^*_{PDV} - T^*_{Non-PDV} \right) / T^*_{Non-PDV} \right\} \times 100$. Table 2 shows the values of R_{T^*} for different values G and c^* with l^*, N, K and h^*_3.

Table 2: Variation of R_{W^*} and R_{T^*} with G for different values c^* with $l^* = 0.3$, $N = 0.3$, $h^*_1 = 1.2$, $K = 0.6$, $h^*_3 = 0.2$ and $h^*_f = 0.6$.

G	c^*	R_{W^*}		R_{T^*}	
		Radial	**Azimuthal**	**Radial**	**Azimuthal**
0	0.2	0.01011370	-0.0404288	0.0260277	0.0270825
	0.4	0.00953117	-0.0398012	0.0255942	0.0299326
	0.6	0.00927388	-0.0382904	0.0249439	0.0353761
0.02	0.2	2.04833	2.06187	5.71249	5.9629
	0.4	1.99477	2.21504	5.6293	6.68584
	0.6	1.91174	2.52222	5.5005	8.05252
0.04	0.2	4.22566	4.31207	12.7855	13.4235
	0.4	4.11217	4.63973	12.5849	15.3255
	0.6	3.93588	5.30107	12.2763	19.1141

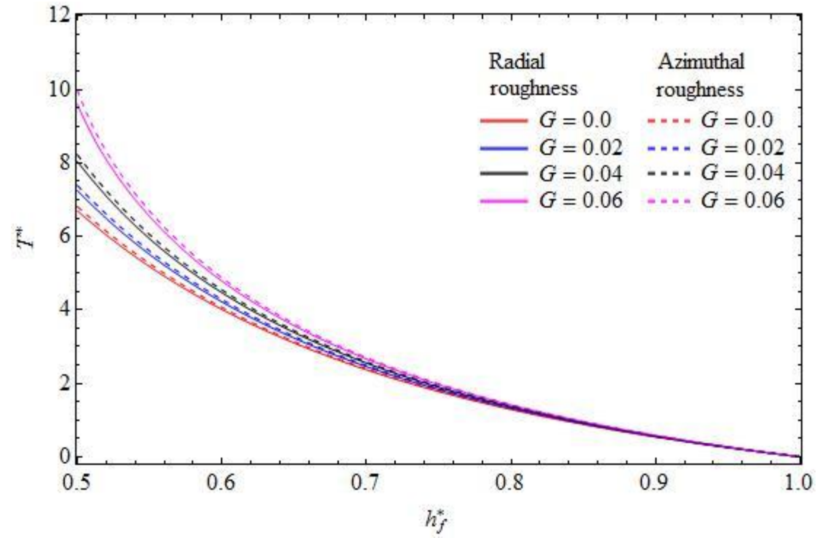

Figure 12: Variation of non-dimensional squeeze film time T^* with h_f^* for different values of G with $l^* = 0.2, K = 0.7, c^* = 0.1, h_3^* = 0.2, N = 0.3$.

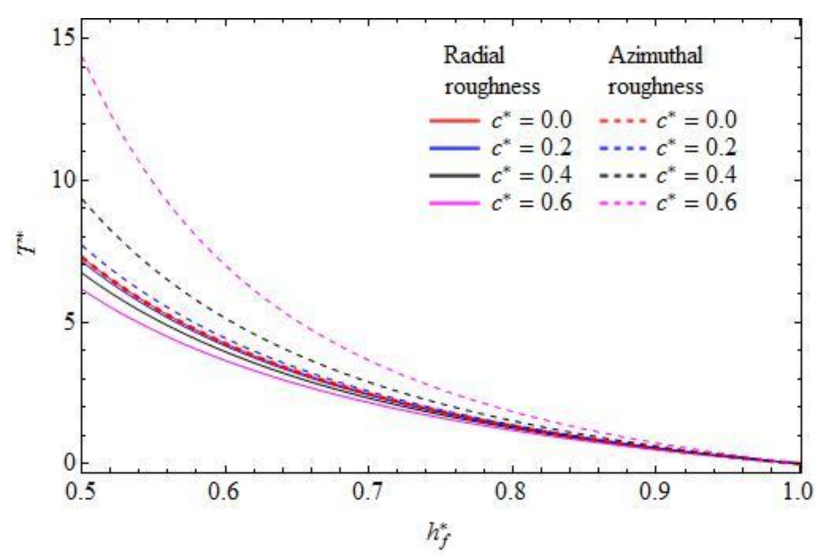

Figure 13: Variation of non-dimensional squeeze film time T^* with h_f^* for different values of c^* with $l^* = 0.2, K = 0.7, h_3^* = 0.2, N = 0.3, G = 0.02$.

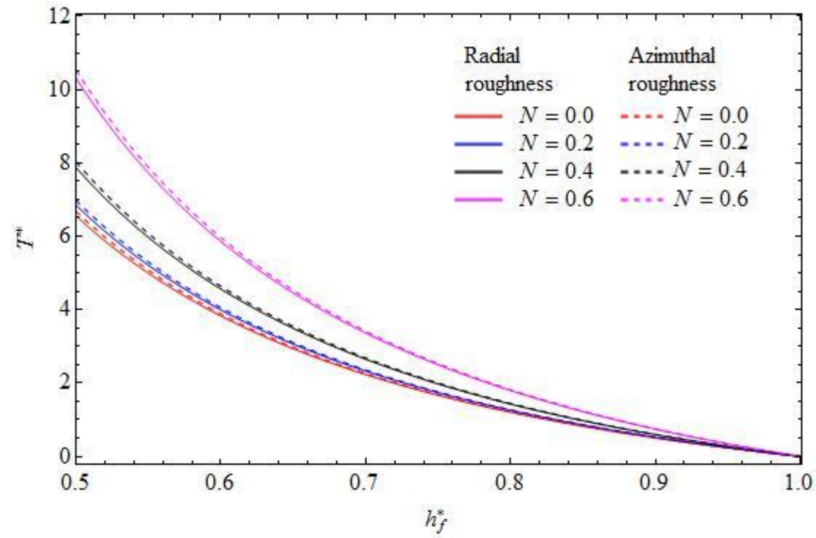

Figure 14: Variation of non-dimensional squeeze film time T^* with h_f^* for different values of N with $l^* = 0.2, K = 0.7, c^* = 0.1, h_3^* = 0.2, G = 0.02$.

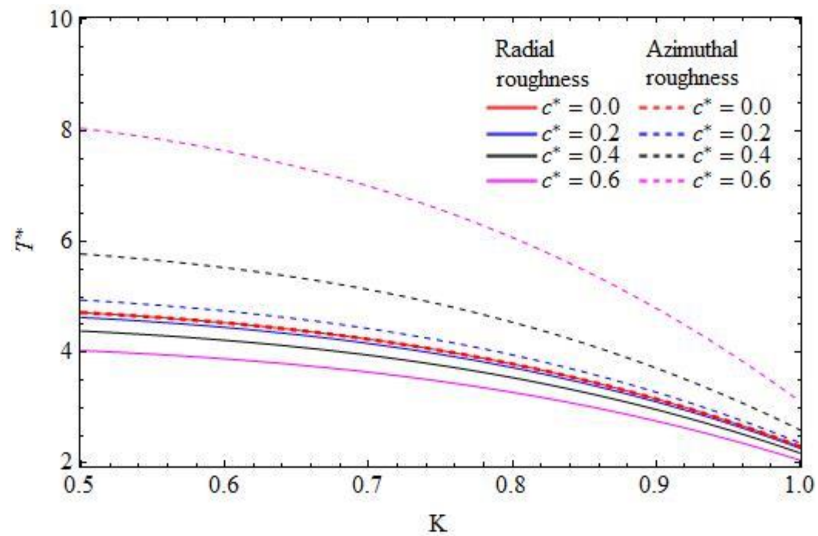

Figure 15: Variation of non-dimensional squeeze film time T^* with K for different values of c^* with $l^* = 0.2, G = 0.02, N = 0.3, h_3^* = 0.2, h_f^* = 0.6$.

CONCLUSIONS

Based on the analysis of pressure distributions, the following important conclusions were drawn:

(a) The effect of pressure-dependent viscosity provides an increase in the pressure, load carrying capacity and squeeze film time for the circular stepped plates as compared to iso-viscous lubricant case.
(b) The one-dimensional azimuthal (radial) roughness patters on the circular stepped plates increases (decreases) the load-carrying capacity and squeeze film time as compared to the corresponding smooth case $(c^{*}=0)$.
(c) The maximum pressure, load carrying capacity and the squeeze film time decreases with increasing values of K.
(d) The dimensionless pressure, load carrying capacity and squeeze film time increases with increasing values of viscosity parameter G, coupling parameter N and micropolar parameter l^{*}.
(e) The results are validated with the available results in the literature and found to be good improvement as per the stochastic theory of lubrication is concerned.

REFERENCES

Bartz, W. J. and Ether, J. (2008) 'Influence of pressure viscosity oils on pressure, temperature and film thickness in elastohydrodynamically lubricated rolling contacts', Proceedings of the Institution of Mechanical Engineers-Part C: Mechanical Engineering Science, Vol. 222, pp. 1271-1280

Barus, C. (1893) 'ART. X.-Isothermals, isopiestics and isometrics relative to viscosity', American Journal of Science (1880-1910), Vol. 45 No. 266, pp. 87-96

Christensen, H. (1969) 'Stochastic models for hydrodynamic lubrication of rough surfaces', Proceedings of the Institution of Mechanical Engineers, Vol.184 No. 1, pp.1013–1026

Christensen, H. and Tonder, K. (1971) 'The hydrodynamic lubrication of rough bearing surfaces of finite width', Journal of Lubrication Technology, Vol. 93 No. No. 3, pp. 324-329

Elsharkawy, A. A. and Al-Fadhalah, K. J. (2011) 'Squeeze film characteristics between a sphere and a rough porous flat plate with micropolar fluids', Lubrication Science, Vol. 23 No. 1, pp. 1-18

Eringen, A. C. (1966) 'Theory of micropolar fluids', Journal of Mathematics and Mechanics, Vol. 16, pp. 1-18

Hanumagowda, B. N. (2015) 'Combined effect of pressure-dependent viscosity and couple stress on squeeze film lubrication between circular step plates', Proceedings of the Institution of Mechanical Engineers, Part J: Journal of Engineering Tribology, Vol. 229 No. 9, pp. 1056-1064

Hanumagowda, B. N., Raju, B. T., Santosh Kumar, J. and Vasanth, K. R. (2018) 'Combined effect of surface roughness and pressure-dependent viscosity over couple stress squeeze film lubrication between circular stepped plates', Proceedings of the Institution of Mechanical Engineers, Part J: Journal of Engineering Tribology, Vol. 232 No. 5 , pp. 525-534

Hanumagowda, B. N., Raju, B. T., Santosh Kumar, J. and Vasanth, K. R. (2018), 'Effect of pressure dependent viscosity on couple stress squeeze film lubrication between porous circular stepped plates' in NCMTA 2018: Journal of Physics: Conference Series, IOP Publishing, Vol. 1000, No. 1, pp. 012081

Hanumagowda, B. N., Shivakumar, H. M., Raju, B. T. and Santosh Kumar, J. (2016) 'Combined effect of pressure dependent viscosity and micropolar fluids on squeeze film circular stepped plates', International Journal of Mathematics Trends and Technology, Vol. 37 No. 3, pp. 175-183

Lin, J. R., Kuo, C. C., Liao, W. H. and Yang, C. B. (2012) 'Non-Newtonian micropolar fluid squeeze film between conical plates', Zeitschrift für Naturforschung A, Vol. 27a No. (6-7), pp. 333-337

Lin, J. R., Liang, L. J. and Chu, L. M. (2010) 'Effects of non-Newtonian micropolar fluids on the squeeze film characteristics between a sphere and a plate surface', Proceedings of the Institution of Mechanical Engineers, Part J: Journal of Engineering Tribology, Vol. 224 No. 8, pp. 825-832

Naduvinamani, N. B and Marali, G. B. (2007) 'Dynamic Reynolds equation for micropolar fluids and the analysis of plane inclined slider bearings with squeezing effect', Proceedings of the Institution of Mechanical Engineers, Part J: Journal of Engineering Tribology, Vol. 221 No. 7, pp. 823-829

Naduvinamani, N. B. and Siddangouda, A. (2009) 'Squeeze film lubrication between circular stepped plates of couple stress fluids', Journal of the Brazilian Society of Mechanical Sciences and Engineering, Vol.31 No.1, pp. 21-26

Naduvinamani, N. B. and Siddangouda, A. (2010) 'On the performance of rough inclined stepped composite bearing with micropolar fluid', Journal of Marine Science and Technology, Vol. 18 No. 2, pp. 233-242

Naduvinamani, N. B., Hanumagowda, B. N. and Fathima, S. T. (2012) 'Combined effects of MHD and surface roughness on the couple stresses squeeze film lubrication between porous circular stepped plates', Tribology International, Vol. 56, pp. 19-29

Naduvinamani, N. B., Santosh, S. and Siddangouda, A. (2010) 'On the squeeze film lubrication of rough short porous partial journal bearings with micropolar fluids', Proceedings of the Institution of Mechanical Engineers, Part J: Journal of Engineering Tribology, Vol. 224 No. 3, pp. 249-257

Naduvinamani, N. B., Siddangouda, A., Kadadi, A. K. and Biradar, S. N. (2015) 'Effect of pressure dependent viscosity on squeeze film characteristics of micropolar fluid in convex curved plates', Tribology-Materials, Surfaces & Interfaces, Vol. 9 No. 3, pp. 154-158

Pinkus, O. and Sternlicht, B. (1961) Theory of hydrodynamic lubrication, McGraw-Hill, New York.

Prakash, J. and Sinha, P. (1975) 'Lubrication theory for micropolar fluids and its application to a journal bearing', International Journal of Engineering Science, Vol. 13 No. 3, pp. 217-232

Rao, P. S., Murmu, B. and Agarwal, S. (2017) 'Effect of surface roughness and non-Newtonian micropolar fluid squeeze film between conical bearings', Zeitschrift für Naturforschung A, Vol. 72 No. 12, pp. 1151-1158

Shukla, J. B. and Isa, M. (1975) 'Generalised Reynolds equation for micropolar lubricants and its application to optimum one-directional slider bearings; effect of solid particles additives in solution', Journal of Mechanical Engineering Science, Vol. 17 No. 5, pp. 280-284

Siddangouda, A., Naduvinamani, N. B. and Kadadi, A. K. (2017) 'Piezo-viscous and surface roughness on the squeeze film characteristics of micropolar fluid in convex curved plates', Journal of Advanced Computing, Vol. 6 No.1, pp. 28-44